RSC Advances

PAPER

View Article Online
View Journal | View Issue

Cite this: *RSC Adv.*, 2026, **16**, 27021

A validated Rhodamine B fluorescence quenching spectrofluorimetric method for solriamfetol determination in human plasma with pharmacokinetic application

Ahmed Serag, *[a] Razaz Abdulaziz Felemban,[bc] Abdulaziz H. Al Khzem,[d] Mansour S. Alturki, [d] Mohammed F. Aldawsari,[e] Manal E. Alosaimi,[f] Maram H. Abduljabbar[g] and Atiah H. Almalki*[hi]

Solriamfetol, a schedule IV wake-promoting agent, represents a significant analytical target requiring sensitive and reliable methods for its quantification in biological matrices. Herein, the fluorescence quenching of Rhodamine B upon interaction with solriamfetol's protonated amine was exploited for the first time for its spectrofluorimetric determination in human plasma. The spectroscopic properties of the analyte–fluorophore system were systematically investigated using absorption and emission spectroscopy, revealing a quenching behavior of Rhodamine B at 578 nm upon interaction with solriamfetol. Subsequently, mechanistic elucidation through Stern–Volmer analysis established static quenching (K_{sv} = 7.95 × 10^5 L mol^{-1}) with thermodynamically favorable interaction (ΔG = −33.66 kJ mol^{-1}) and 1 : 1 stoichiometry *via* Job's method. Furthermore, quantum mechanical calculations confirmed electrostatic complementarity between solriamfetol's protonated amine and Rhodamine B's carboxylate moiety. Experimental parameters were optimized *via* sequential univariate approaches. Method validation was conducted according to ICH M10 guidelines demonstrating excellent analytical performance with linearity across 25.0–1000.0 ng mL^{-1} concentration range (r^2 = 0.9991), high sensitivity (LOD = 8.05 ng mL^{-1}, LOQ = 24.38 ng mL^{-1}), and precision (% RSD < 4.56%). Analytical equivalence with LC-MS/MS was further confirmed through cross-validation studies. Finally, the method was successfully implemented for pharmacokinetic profiling in human volunteer plasma following administration of 75 mg solriamfetol, yielding $t_{1/2}$ = 7.6 h, C_{max} = 465 ng mL^{-1}, and t_{max} = 1.5 h in agreement with literature values. This methodology offers significant advantages including visible-wavelength excitation minimizing matrix interference, rapid analysis time, and reduced environmental impact compared to conventional chromatographic techniques, thus providing a viable alternative for solriamfetol determination in therapeutic drug monitoring and pharmacokinetic profiling applications.

Received 23rd March 2026
Accepted 12th May 2026

DOI: 10.1039/d6ra02388f

rsc.li/rsc-advances

1. Introduction

Solriamfetol hydrochloride ([*R*]-2-amino-3-phenylpropylcarbamate hydrochloride), a phenylpropylamine derivative, has emerged as a clinically significant pharmacotherapeutic agent for the management of excessive daytime somnolence in narcolepsy and obstructive sleep apnea (OSA) populations.[1,2] Mechanistically, this compound exhibits dual inhibitory activity at catecholaminergic neurotransmitter transporters with micromolar potency, demonstrating IC_{50} values of 2.9 μM and 4.4 μM for dopamine transporter and norepinephrine transporter, respectively, while exhibiting negligible affinity for serotonergic systems (IC_{50} > 100 μM).[3] In contradistinction to classical sympathomimetic agents, solriamfetol demonstrates minimal monoamine-releasing properties, potentially accounting for its differentiated

[a]*Pharmaceutical Analytical Chemistry Department, Faculty of Pharmacy, Al-Azhar University, Nasr City, 11751, Cairo, Egypt. E-mail: Ahmedserag777@hotmail.com*
[b]*Department of Basic Medical Sciences, College of Medicine, King Saud Bin Abdulaziz University for Health Sciences, Jeddah, Saudi Arabia*
[c]*King Abdullah International Medical Research Centre, Jeddah, Saudi Arabia*
[d]*Department of Pharmaceutical Chemistry, College of Pharmacy, Imam Abdulrahman Bin Faisal University, Dammam, Saudi Arabia*
[e]*Department of Pharmaceutics, College of Pharmacy, Prince Sattam Bin Abdulaziz University, Al-kharj, 11942, Saudi Arabia*
[f]*Department of Basic Sciences, College of Medicine, Princess Nourah Bint Abdulrahman University, P. O. Box 84428, Riyadh, 11671, Saudi Arabia*
[g]*Department of Pharmacology and Toxicology, College of Pharmacy, Taif University, P. O. Box 11099, Taif, 21944, Saudi Arabia*
[h]*Addiction and Neuroscience Research Unit, Health Science Campus, Taif University, P. O. Box 11099, Taif, 21944, Saudi Arabia. E-mail: ahalmalki@tu.edu.sa*
[i]*Department of Pharmaceutical Chemistry, College of Pharmacy, Taif University, P. O. Box 11099, Taif, 21944, Saudi Arabia*

neuropsychopharmacological profile.[3] Solriamfetol undergoes minimal hepatic biotransformation, with approximately 90% of the administered dose excreted unchanged in urine within 48 hours, rendering renal clearance the predominant elimination pathway.[4] Administration of high-fat meals delays T_{max} by approximately 1 hour without significantly altering bioavailability or maximum plasma concentration (C_{max}).[5] In patients with compromised renal function, geometric mean AUC increases proportionally to renal impairment severity (53%, 129%, and 339% for mild, moderate, and severe impairment, respectively) necessitating dosage adjustment.[4]

The clinical significance of solriamfetol derives from the substantial prevalence of excessive daytime sleepiness in sleep disorder populations, affecting 9–38% of the general population.[6,7] Phase III randomized controlled trials have demonstrated significant improvements in objective parameters and subjective assessments compared with placebo.[2,8] Despite its therapeutic utility, the schedule IV controlled substance classification of solriamfetol highlights the need for validated analytical methods for its determination in biological matrices, supporting applications in therapeutic drug monitoring, pharmacokinetic profiling, pharmaceutical quality control, and forensic toxicology.[9]

Literature review revealed a limited number of analytical methods for solriamfetol quantification, each presenting significant limitations that constrain their application. Chromatographic methods include a chiral HPLC approach for separating solriamfetol enantiomers, which helps distinguish between the active *R*-form and inactive *S*-form of the drug.[10] However, this method requires specialized columns and consumes large amounts of organic solvents, making it less environmentally friendly. Another chromatographic technique, UPLC-UV, was developed for quality control to identify and measure eight different impurities in solriamfetol products.[11] While effective for impurity profiling, this method relies on gradient elution and uses potentially hazardous perchloric acid in the mobile phase, raising safety concerns. For maximum sensitivity in biological samples, an LC-MS/MS method was developed that can detect extremely small amounts of solriamfetol (as low as 11.12 pg mL^{-1}) in plasma, making it valuable for pharmacokinetic studies.[12] Despite its excellent sensitivity, this approach requires expensive equipment, specialized training, and complex sample preparation including protein precipitation steps, limiting its accessibility for routine use. A capillary electrophoresis method was created for simultaneous separation of solriamfetol and phenylalaninol enantiomers.[13] Although this technique uses minimal solvents and achieves separation within 7 minutes, it suffers from lower sensitivity, limited sample capacity, and requires specialized equipment, restricting its widespread application.

On the other hand, fluorescence spectroscopy offers several important advantages as an analytical technique compared to other methods. It provides excellent sensitivity allowing for detection of very low concentrations of the analyte.[14,15] The technique uses relatively simple and affordable instruments that are commonly available in most laboratories.[16,17] Moreover, fluorescence methods consume much less organic solvent than chromatographic techniques, making them more environmentally friendly and cost-effective.[18,19] For solriamfetol analysis, only one spectrofluorimetric method has been reported in the literature.[9] This method measures the drug's intrinsic fluorescence at 522 nm following excitation at 260 nm in ammonium acetate buffer (pH 4). The approach achieves good sensitivity and very low detection and quantification limits; however, the method comes with considerable limitations. The excitation at 260 nm falls within a spectral region where many biological components naturally fluoresce, compromising selectivity in complex matrices. While effective for urine analysis, the method struggles with plasma samples due to interference from protein autofluorescence. Other limitations include fluorescence intensity variations with pH changes, requiring strict buffer control and potential photodegradation during analysis. These limitations highlight the need for developing alternative spectrofluorimetric approaches with improved selectivity characteristics, potentially through fluorescence derivatization strategies or longer-wavelength excitation parameters that minimize biological matrix interference.

Fluorescent probes have emerged as powerful analytical tools for the detection and quantification of various analytes, offering versatility across diverse applications ranging from pharmaceutical analysis to environmental monitoring.[20] Among various fluorescent probes, Rhodamine B offers several important advantages: (1) it exhibits high brightness and stability under various conditions, making measurements more reliable;[21] (2) it requires excitation with visible light rather than UV light, which significantly reduces background interference from biological components that naturally fluoresce in the UV region; (3) its zwitterionic carboxylate moiety engages in selective electrostatic interactions with protonated amine groups of basic drug molecules, leading to stable ground-state complex formation that produces a concentration-dependent decrease in fluorescence intensity, providing a sensitive measurement basis,[22] and (4) the large difference between its excitation and emission wavelengths makes it easier to distinguish the signal from background noise. These properties make Rhodamine B particularly promising for developing improved methods for solriamfetol detection in complex biological samples like plasma.

Therefore, the present study aimed to develop a novel, sensitive, and selective spectrofluorimetric method for solriamfetol determination in plasma based on its quenching effect on Rhodamine B fluorescence. Initially, spectral characteristics of both solriamfetol and Rhodamine B were thoroughly investigated using UV-visible and fluorescence spectroscopy. Furthermore, the mechanism of quenching was comprehensively characterized through Stern–Volmer analysis, thermodynamic studies, Job's method, and quantum mechanical calculations to identify the forces governing the quenching interaction between solriamfetol and Rhodamine B. Additionally, optimization of experimental variables affecting the quenching process was systematically investigated. Moreover, the method was fully validated according to ICH M10 guidelines to ensure reliability for clinical and forensic applications. In addition, practical applications to pharmacokinetic profiling in

human plasma samples were demonstrated thereby providing a complete evaluation of the method's utility for therapeutic drug monitoring and anti-doping surveillance programs.

2. Experimental

2.1. Materials and reagents

Solriamfetol hydrochloride reference standard (purity 99.9%) was procured from Sigma-Aldrich (St. Louis, MO, USA). Rhodamine B (analytical grade, dye content ≥95%) was also supplied by Sigma-Aldrich (St. Louis, MO, USA). For buffer preparation, analytical grade components including boric acid, glacial acetic acid, and phosphoric acid were utilized for Britton–Robinson buffer formulation from El-Nasr Pharmaceutical Chemicals Co, Cairo, Egypt. HPLC grade acetonitrile was purchased from Merck (Darmstadt, Germany). All other employed chemicals and solvents were of analytical reagent grade and were used without further purification. Double-distilled water was exclusively employed for all solution preparations and dilutions throughout the experimental work.

Stock standard solution of solriamfetol (1.0 mg mL^{-1}) was prepared by dissolving an accurately weighed amount of solriamfetol hydrochloride reference standard in double-distilled water. Working standard solutions were freshly prepared by serial dilution of the stock solution with double-distilled water to achieve the required concentration range of 25.0–1000.0 ng mL^{-1}. Rhodamine B stock solution (0.01% w/v) was prepared by dissolving 20 mg of Rhodamine B in 100 mL of double-distilled water and stored in an amber volumetric flask at 4 °C, protected from light exposure to prevent photodegradation. All stock solutions were stable for at least one week when stored at 4 °C protected from light. Britton–Robinson buffer solutions spanning pH 3.0–9.0 were prepared by combining equimolar (0.04 M) concentrations of boric acid, glacial acetic acid, and phosphoric acid, with subsequent pH adjustment using 0.2 M sodium hydroxide solution to achieve the desired pH values.

2.2. Instrumentation

Fluorescence measurements were conducted using a Jasco FP-6200 spectrofluorometer (Tokyo, Japan) equipped with a 150 W xenon lamp as the excitation source. Quartz cells with 1.0 cm path length were utilized for all spectrofluorimetric measurements. The excitation and emission monochromator slit widths were optimized at 5 nm to achieve maximum sensitivity while maintaining acceptable signal-to-noise ratio. UV-visible absorption spectra were recorded using a Shimadzu UV-1800 double-beam spectrophotometer (Kyoto, Japan) with matched 1.0 cm quartz cells. pH measurements were performed using a Jenway 3510 pH meter (Stone, Staffordshire, UK) equipped with a combined glass electrode. The instrument was calibrated daily using standard buffer solutions of pH 4.0, 7.0, and 10.0. Centrifugation of plasma samples was accomplished using a refrigerated centrifuge (Hermle Z326K, Wehingen, Germany) maintained at 4 °C.

2.3. General procedure for fluorescence quenching measurements

The fluorescence quenching methodology involves monitoring the decrease in Rhodamine B fluorescence intensity upon interaction with varying concentrations of solriamfetol. In a series of 10 mL volumetric flasks, a fixed volume (1.0 mL) of 0.01% w/v Rhodamine B solution was transferred, followed by the addition of 1.5 mL of Britton–Robinson buffer (pH 6.0). Varying volumes of the solriamfetol working standard solutions were subsequently added to these flasks, and the final volume was adjusted to 10 mL with double-distilled water. The order of addition was maintained consistently throughout all experiments to ensure reproducibility. The solutions were thoroughly mixed and allowed to equilibrate at ambient temperature (25 ± 2 °C) for 3 minutes prior to fluorescence measurement.

Fluorescence measurements were conducted at optimized excitation and emission wavelengths of 554 nm and 578 nm, respectively, with excitation and emission slit widths set at 5 nm. The fluorescence intensity of Rhodamine B was observed to decrease proportionally with increasing solriamfetol concentration, forming the basis for quantitative determination. The ratio of fluorescence intensity (F_0/F) was plotted against solriamfetol concentration to establish the analytical calibration curve, where F_0 and F represent the fluorescence intensities of Rhodamine B in the absence and presence of solriamfetol, respectively. All measurements were performed in triplicate ($n = 3$) and results are expressed as mean ± standard deviation.

2.4. Optimization of experimental conditions

Detailed optimization of various parameters including pH of buffer, buffer volume, Rhodamine B volume and reaction time are presented in the SI.

2.5. Quantum mechanical calculations

Quantum mechanical calculations were performed to elucidate the molecular interaction mechanism between solriamfetol and Rhodamine B using Gaussian 09 software package (Gaussian, Inc., Wallingford, CT, USA). Geometry optimizations were conducted using the RPM3 semi-empirical method, which provides an optimal balance between computational efficiency and accuracy for large molecular systems. Initial molecular structures were constructed using GaussView 6.0 software and optimized without symmetry constraints. Vibrational frequency calculations were performed at the same level of theory to confirm the absence of imaginary frequencies and to obtain thermodynamic parameters.

The binding energy (ΔE) of the solriamfetol–Rhodamine B complex was calculated according to the following equation:

$$\Delta E = E(\text{complex}) - [E(\text{solriamfetol}) + E(\text{Rhodamine B})]$$

where E(complex), E(solriamfetol), and E(Rhodamine B) represent the electronic energies of the optimized complex, solriamfetol, and Rhodamine B, respectively. The optimized geometries and electronic properties of solriamfetol,

Rhodamine B, and their complex were comprehensively analyzed to understand the nature of the fluorescence quenching mechanism.

2.6. Method validation

The validation of the proposed spectrofluorimetric method was performed according to the International Council for Harmonization (ICH) M10 guidelines for bioanalytical method validation.[23] A comprehensive validation protocol was implemented to ensure analytical reliability and applicability for quantitative determination of solriamfetol in pharmaceutical formulations and biological matrices. Details about the sample preparation protocol and various validation parameters including linearity, sensitivity, selectivity, accuracy, precision and robustness are presented in the SI.

2.7. Pharmacokinetics studies

The pharmacokinetic study was conducted in accordance with the Declaration of Helsinki and was approved by the Ethics Committee of the Faculty of Medicine, Al-Azhar University, Damietta branch (approval no. DFM-IRB00012367-25-04-029), Egypt. Five healthy male volunteers (age range: 25–45 years; weight range: 65–80 kg) participated in the study after providing written informed consent. Following an overnight fast, each volunteer received a single oral dose of 75 mg solriamfetol with 240 mL of water. Blood samples (5 mL) were collected into heparinized tubes at predetermined time intervals (0, 0.5, 1, 1.5, 2, 3, 3.5, 4, 6, 8, 12 and 24 h) post-dose. Plasma was immediately separated by centrifugation at 3500 rpm for 10 minutes and stored at −20 °C until analysis.

Pharmacokinetic parameters were calculated using non-compartmental analysis with PKSolver software.[24] The parameters evaluated included maximum plasma concentration (C_{max}), time to reach maximum concentration (t_{max}), elimination half-life ($t_{1/2}$), area under the plasma concentration–time curve from zero to the last measurable concentration ($AUC_{0\rightarrow t}$), area under the curve from zero to infinity ($AUC_{0\rightarrow\infty}$), apparent volume of distribution (V_z/F), and apparent clearance (CL/F).

3. Results and discussion

3.1. Spectral characteristics of Rhodamine B and solriamfetol

The spectral properties of Rhodamine B and its interaction with solriamfetol were thoroughly investigated using UV-visible absorption and fluorescence spectroscopy to establish the physicochemical basis for the analytical methodology (Fig. 1). The UV-visible absorption spectrum of Rhodamine B exhibited a characteristic absorption maximum at 554 nm (Fig. 1A), attributable to the $\pi \rightarrow \pi^*$ electronic transitions of the xanthene chromophore. This spectral profile aligns with the predominant zwitterionic form ($R\pm$) of Rhodamine B expected at the optimized pH, where the equilibrium strongly favors the open, colored structure rather than the colorless lactone form. The spectroscopic behavior observed is consistent with established literature on Rhodamine B, where the zwitterionic species predominates at pH values between 4.0 and 10.0, exhibiting intense absorption in the visible region with molar extinction coefficients approaching 10^5 M^{-1} cm^{-1}. Upon addition of solriamfetol, a distinct spectral modification was observed, characterized by increased absorbance and a slight bathochromic shift (Fig. 1A), suggesting perturbation of the electronic transitions within the Rhodamine B chromophore upon interaction with solriamfetol.

The fluorescence emission spectrum of Rhodamine B, excited at 554 nm, exhibited a strong emission peak at 578 nm with a Stokes shift of 24 nm (Fig. 1B). This relatively small Stokes shift is characteristic of rigid fluorophore structures with minimal geometric reorganization between ground and excited states, offering excellent spectral resolution for analytical applications. The observed excitation–emission profile demonstrates optimal spectral separation with minimal overlap, facilitating precise fluorometric measurements and enhancing method sensitivity by maximizing signal-to-noise ratio.[21] The intense fluorescence emission is characteristic of Rhodamine B's xanthene moiety, which possesses a high quantum yield in aqueous solutions due to restricted intramolecular rotation and diminished non-radiative decay pathways. The addition of increasing concentrations of solriamfetol resulted in progressive reduction of fluorescence intensity without alteration of the spectral profile or emission maximum wavelength (Fig. 1C). This concentration-dependent quenching behavior provides initial evidence for a specific interaction between Rhodamine B and solriamfetol, prompting further mechanistic investigation through Stern–Volmer analysis, thermodynamic studies, Job's method, and quantum mechanical calculations as described in the following section.

3.2. Quenching mechanism investigation

3.2.1. Stern–Volmer analysis. The fluorescence quenching mechanism between Rhodamine B and solriamfetol was systematically investigated using Stern–Volmer analysis at multiple temperatures (298, 303, and 313 K) to elucidate the nature of the interaction and derive quantitative thermodynamic parameters. The Stern–Volmer analysis was conducted under pseudo-first-order conditions, wherein the Rhodamine B concentration (2.09×10^{-5} M) substantially exceeded the solriamfetol concentration range (4.33×10^{-7} to 4.33×10^{-6} M) throughout the analytical range, representing a 5 to 48-fold molar excess of fluorophore over analyte, ensuring that the fluorophore concentration remained effectively constant during the quenching interaction. The Stern–Volmer plots, constructed by plotting the fluorescence intensity ratio (F_0/F) against solriamfetol concentration, exhibited excellent linearity across the investigated concentration range at all temperatures examined (Fig. 2A). The Stern–Volmer quenching constants (K_{sv}) were determined to be 7.95×10^5, 7.25×10^5, and 6.19×10^5 L mol^{-1} at 298, 303, and 313 K, respectively (Table S1). The systematic decrease in K_{sv} values with increasing temperature provides strong supplementary evidence for static quenching as the predominant mechanism, as dynamic quenching processes invariably exhibit the opposite temperature dependence due to

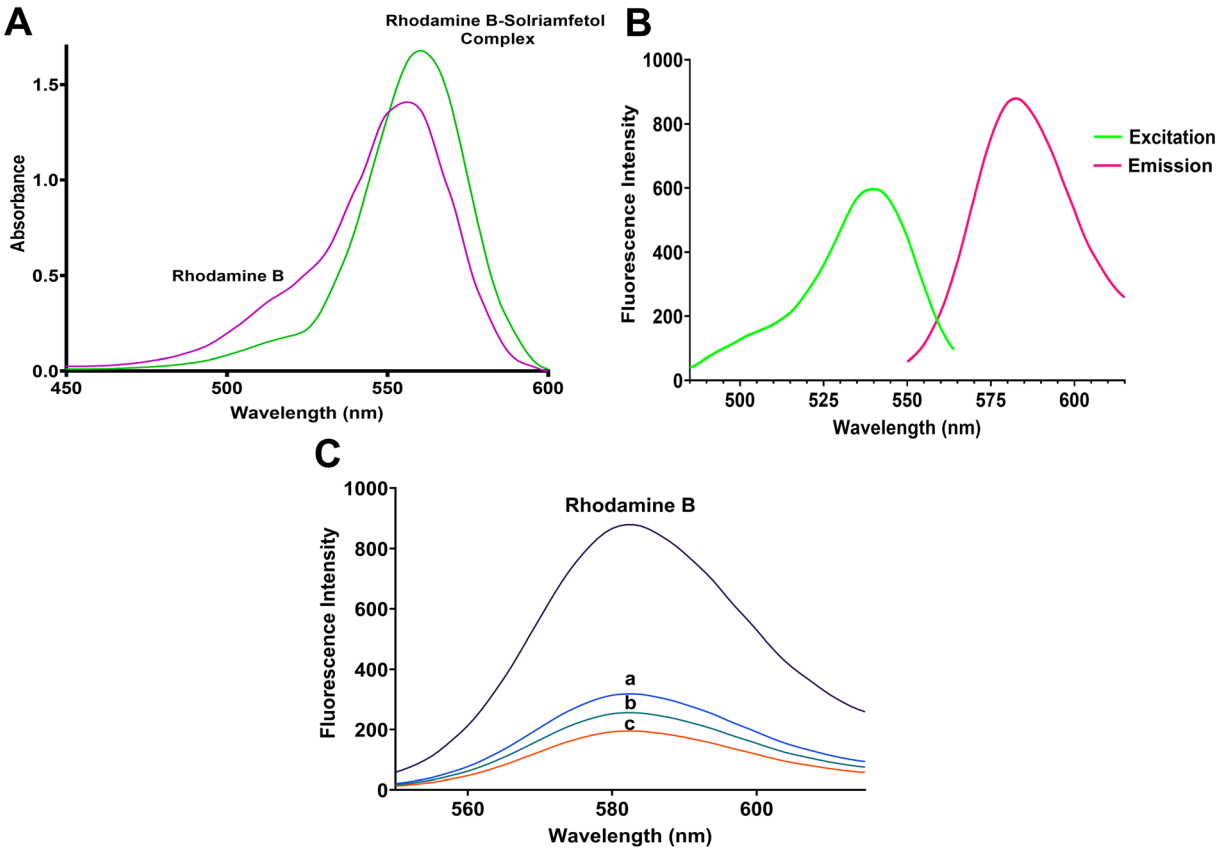

Fig. 1 (A) Absorption spectral profiles of Rhodamine B in the absence and presence of solriamfetol exhibiting hyperchromic effect at λ_{max} 554 nm in aqueous Britton–Robinson buffer (pH 6.0), indicating perturbation of electronic transitions within the xanthene chromophore upon formation of the ground-state complex. (B) Excitation–emission spectral characterization of Rhodamine B demonstrating maximum excitation efficiency at 554 nm and corresponding fluorescence emission at 578 nm with characteristic Stokes shift of 24 nm in aqueous Britton–Robinson buffer (pH 6.0). (C) Progressive quenching of Rhodamine B fluorescence emission intensity upon sequential addition of increasing solriamfetol concentrations: (a) 500 ng mL^{-1}, (b) 700 ng mL^{-1}, and (c) 1000 ng mL^{-1} at pH 6.0, demonstrating the turn-off fluorescence sensing mechanism.

enhanced molecular diffusion at elevated temperatures. The magnitude of the K_{sv} values in the order of 10^5 L mol^{-1} further corroborates this assignment, as dynamic quenching constants are typically two to three orders of magnitude lower (10^2 to 10^3 L mol^{-1}) due to diffusion-limited interactions. Static quenching involves the formation of a non-fluorescent ground-state complex between the fluorophore and quencher, thereby reducing the concentration of free fluorophore available for excitation. The intercept value (1.045), approximating unity, further supports this mechanism and confirms the absence of significant inner-filter effects or other interfering phenomena in the experimental system.

The association constant (K_a) was determined using the modified Stern–Volmer equation:

$$F_0/(F_0 - F) = 1 + 1/(K_a[Q])$$

where F_0 and F represent the fluorescence intensities in the absence and presence of solriamfetol, respectively, and [Q] denotes the solriamfetol concentration. The association constants were determined to be 9.25×10^5, 8.23×10^5, and 6.59×10^5 L mol^{-1} at 298, 303, and 313 K, respectively, with the decreasing K_a values at elevated temperatures further corroborating the static quenching mechanism and confirming the formation of a stable ground-state Rhodamine B–solriamfetol complex. The consistency between K_{sv} and K_a values at all temperatures further validates the proposed static quenching mechanism and provides a reliable foundation for subsequent thermodynamic analysis.

3.2.2. Thermodynamic analysis. The thermodynamic parameters governing the Rhodamine B–solriamfetol interaction were calculated from the temperature-dependent association constants using van't Hoff analysis to elucidate the fundamental forces driving complex formation. The Gibbs free energy change (ΔG) was determined at each temperature using the equation:

$$\Delta G = -RT \ln K_a$$

where R represents the universal gas constant (8.314 J mol^{-1} K^{-1}), T denotes the absolute temperature, and K_a is the association constant derived from the modified Stern–Volmer analysis at each temperature. The ΔG values were calculated to be −34.05, −34.33, and −34.88 kJ mol^{-1} at 298, 303, and 313 K,

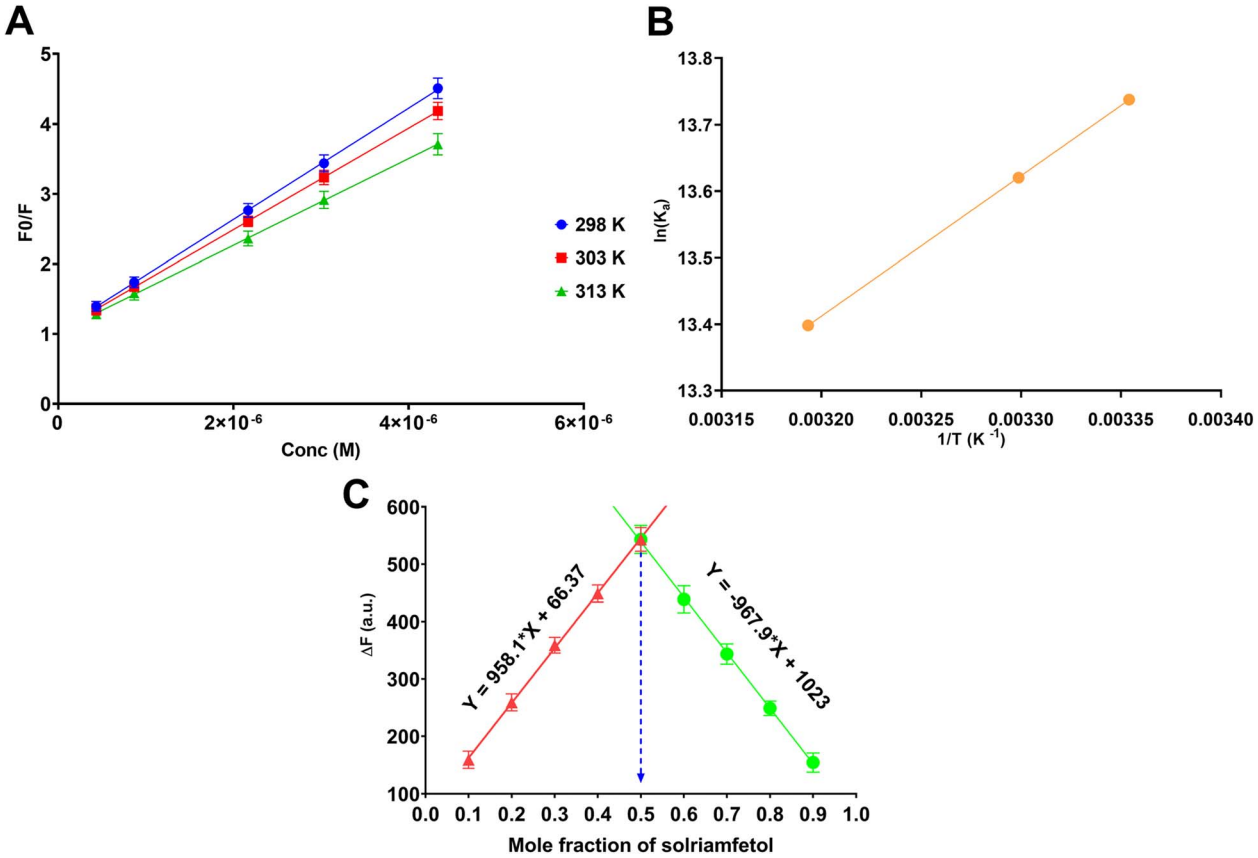

Fig. 2 (A) Stern–Volmer plots of F_0/F *versus* solriamfetol molar concentration at 298 K (●), 303 K (■), and 313 K (▲) in Britton–Robinson buffer (pH 6.0); the systematically decreasing K_{sv} values with increasing temperature confirm static quenching as the predominant mechanism; error bars represent standard deviation of triplicate measurements. (B) van't Hoff plot of $\ln(K_a)$ *versus* $1/T$ yielding $\Delta H = -17.57$ kJ mol^{-1} and $\Delta S = +55.27$ J mol^{-1} K^{-1}, confirming spontaneous exothermic complex formation driven by electrostatic interactions. (C) Job's continuous variation plot for determination of Rhodamine B–solriamfetol complex stoichiometry demonstrating maximum fluorescence intensity change (ΔF) at mole fraction 0.5, confirming 1 : 1 binding ratio.

respectively, with the increasingly negative values confirming enhanced thermodynamic favorability of the Rhodamine B–solriamfetol interaction at elevated temperatures. The van't Hoff plot of $\ln(K_a)$ *versus* $1/T$ yielded an excellent linear relationship (Fig. 2B), from which the enthalpy change ($\Delta H = -17.57$ kJ mol^{-1}) and entropy change ($\Delta S = +55.27$ J mol^{-1} K^{-1}) were derived (Table S1).

According to the Ross and Subramanian classification framework for non-covalent binding forces, the combination of negative ΔH and positive ΔS is characteristic of electrostatic interactions as the predominant driving force for complex formation. The negative ΔH confirms the exothermic nature of the binding interaction, while the positive ΔS reflects favorable reorganization of solvent molecules upon complex formation, collectively contributing to the spontaneity of the interaction. This thermodynamic profile is fully consistent with the molecular structures of both compounds, where the electrostatic complementarity between the carboxylate moiety of Rhodamine B and the protonated amine group of solriamfetol drives strong non-covalent complex formation.

3.2.3. Job's continuous variation method. The stoichiometry of the Rhodamine B–solriamfetol complex was determined using Job's continuous variation method (Fig. 2C). Equimolar stock solutions (4.00×10^{-5} M) of Rhodamine B and solriamfetol were mixed in varying volume ratios while maintaining a constant total concentration. The change in fluorescence intensity (ΔF) was plotted against the mole fraction of solriamfetol, yielding a symmetrical curve with an inflection point at 0.5.

The inflection point corresponding to the maximum ΔF value indicates a 1 : 1 stoichiometry for the Rhodamine B–solriamfetol complex. The linear regression plots for the ascending and descending portions of the Job's plot intersect precisely at a mole fraction of 0.5, confirming the equimolar composition of the complex. This stoichiometric ratio provides critical insights into the binding mechanism and facilitates the interpretation of quantum mechanical calculations for the elucidation of specific interaction sites.

The 1 : 1 stoichiometry, combined with the thermodynamic parameters and Stern–Volmer analysis, presents a comprehensive physicochemical foundation for understanding the Rhodamine B–solriamfetol interaction. This molecular-level characterization not only validates the analytical methodology but also provides fundamental insights into the structural

determinants of fluorescence quenching, thereby enabling rational optimization of experimental conditions for maximum analytical sensitivity and selectivity.

3.3. Quantum mechanical calculations

Quantum mechanical calculations were performed to elucidate the structural basis and energetic profile of the Rhodamine B–solriamfetol interaction at the molecular level. The optimized molecular structures of individual compounds and their complex are depicted in Fig. 3. Rhodamine B adopts its characteristic planar xanthene core configuration with diethylamino substituents oriented perpendicular to the main chromophore plane (Fig. 3A). Solriamfetol displays its phenethylamine-derived structure with the carbamate moiety extending from the primary amine (Fig. 3B).

The geometry-optimized complex (Fig. 3C) reveals critical intermolecular interactions governing the fluorescence quenching phenomenon. The primary binding interface involves electrostatic interactions between the protonated amino group of solriamfetol and the carboxylate oxygen of Rhodamine B (3.02 Å). Additionally, hydrogen bonding occurs between a hydrogen atom of solriamfetol and the carbonyl oxygen of the carboxylate group in Rhodamine B (1.77 Å), further stabilizing the complex. The observed molecular orientation corroborates the 1 : 1 stoichiometry determined experimentally *via* Job's method and provides structural validation for the static quenching mechanism proposed from Stern–Volmer analysis.

The energetic parameters derived from the semi-empirical PM3 calculations are summarized in Table 1. The negative binding energy ($\Delta E = -0.041229$ hartree) confirms the thermodynamic favorability of complex formation, consistent with the experimentally determined negative Gibbs free energy. The calculated enthalpy change ($\Delta H = -24.63$ kcal mol^{-1}) indicates an enthalpy-driven association process, while the negative entropy change ($\Delta S = -27.63$ cal mol^{-1} K^{-1}) reflects the decreased molecular freedom upon complex formation.

The electronic properties of the complex demonstrate significant perturbations compared to the constituent molecules. The calculated dipole moment of the complex (8.731191 debye) differs substantially from the algebraic sum of individual dipole moments, with a differential of −1.903303 debye, suggesting significant charge redistribution upon complexation (Table 1). This charge complementarity likely contributes to the stabilization of the ground-state complex. Furthermore, the polarizability increase ($\Delta = 10.462$ au) indicates enhanced

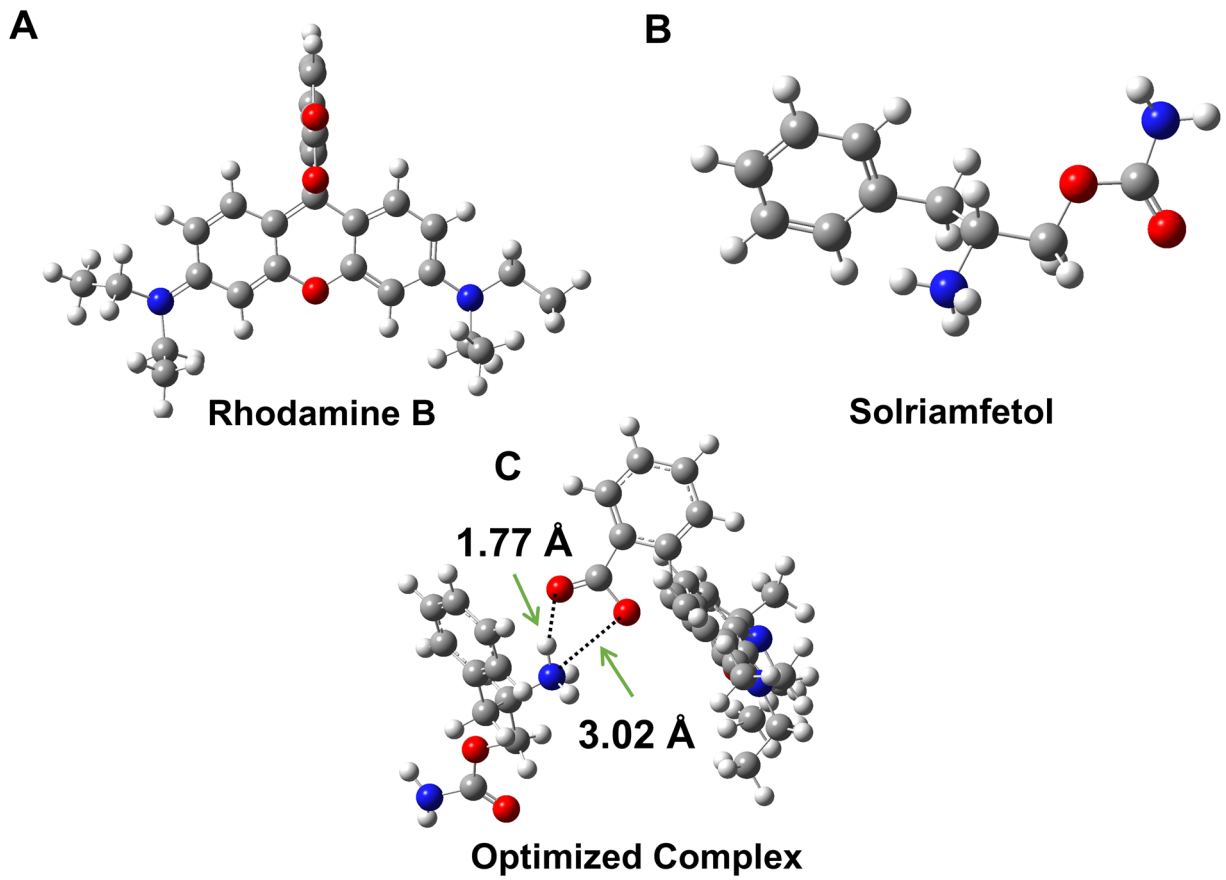

Fig. 3 (A) Geometry-optimized molecular structure of Rhodamine B displaying characteristic planar xanthene core configuration with diethylamino substituents oriented perpendicular to the main chromophore plane. (B) Optimized conformation of solriamfetol revealing the phenethylamine scaffold with carbamate functionality. (C) PM3-minimized structure of the supramolecular complex highlighting critical binding interfaces between solriamfetol's protonated amino group and Rhodamine B's carboxylate group.

Table 1 Computational quantum mechanical parameters quantifying the thermodynamic and electronic properties of Rhodamine B, solriamfetol, and their supramolecular interaction complex obtained *via* semi-empirical PM3 calculations

Parameter	Rhodamine B	Solriamfetol	Complex	Δ (complex − sum)	Interpretation
E(RPM3) (hartree)	−0.075847	0.139372	0.022296	−0.041229	Favorable interaction
Dipole moment (debye)	3.223835	7.410659	8.731191	−1.903303	Charge complementarity
Polarizability (au)	270.792	97.984	379.238	10.462	Electronic delocalization
ΔH (kcal mol^{-1})	—	—	—	−24.63	Enthalpy-driven binding
ΔS (cal mol^{-1} K)	—	—	—	−27.63	Decreased molecular freedom
ΔG (kJ mol^{-1})	—	—	—	−68.6	Strong non-covalent interaction

electronic delocalization within the complex and thereby contributing to fluorescence quenching.

The calculated Gibbs free energy of the complex (ΔG = −68.6 kJ mol^{-1}) exceeds the experimentally determined value (−33.66 kJ mol^{-1}) by approximately twofold. This discrepancy is attributable to two principal factors: (1) the computational model represents gas-phase conditions, neglecting solvent effects that would moderate the interaction strength in aqueous media, and (2) inherent limitations of semi-empirical methods compared to higher-level density functional theory (DFT) calculations. Semi-empirical methods were employed due to computational resource constraints when handling these large molecular systems, providing a reasonable compromise between accuracy and computational efficiency.

The quantum mechanical calculations substantiate the proposed static quenching mechanism by demonstrating the formation of a stable ground-state complex through specific intermolecular interactions. The computational results align with experimental observations and provide atomic-level insights into the structural determinants of the Rhodamine B–solriamfetol interaction, further validating the analytical methodology developed for solriamfetol determination based on fluorescence quenching.

3.4. Optimization of experimental conditions

The optimization of experimental parameters was systematically investigated to maximize the analytical sensitivity of the fluorescence quenching method for solriamfetol determination. A univariate approach was employed to establish optimal conditions for pH, buffer volume, Rhodamine B concentration, and reaction time (Fig. 4).

The influence of pH (3.0–9.0) on quenching efficiency revealed maximum F_0/F ratios at pH 6.0–7.0 (Fig. 4A). At pH 6.0, Rhodamine B (carboxyl pK_a = 3.50, diethylamino pKa ≈ 4.34) predominantly exists in its zwitterionic form (Fig. S1), while solriamfetol maintains protonation of its secondary amine (pK_a ≈ 9.05) with the carbamate group (pK_a ≈ 15.74) remaining unionized (Fig. S2) as calculated by Marvin Sketch software (version 24.3.2, Chemaxon), (https://www.chemaxon.com). This ionic configuration facilitates optimal electrostatic complementarity between Rhodamine B's carboxylate and solriamfetol's protonated amine, enhancing complex stability. Moreover, the diminished quenching efficiency at pH < 5.0 and >7.5 results from unfavorable alterations in these ionization states, disrupting the electrostatic interactions crucial for complex formation.

Additionally, buffer volume optimization (0.5–3.5 mL) demonstrated peak quenching efficiency at 1.5 mL (Fig. 4B). This optimal volume provides sufficient ionic strength to stabilize molecular interactions while avoiding excessive salt concentrations that might disrupt electrostatic forces between the fluorophore and analyte. Furthermore, the observed bell-shaped response curve illustrates the balance between insufficient and excessive buffer capacity, which directly influences the stability of the Rhodamine B–solriamfetol complex.

Rhodamine B concentration was studied by investigating volumes (0.5–3.5 mL) of 0.01% w/v solution, with maximum quenching efficiency observed at 1.0 mL (Fig. 4C). The observed concentration-dependency reflects equilibrium dynamics between fluorophore and quencher. Suboptimal quenching at lower concentrations stems from insufficient fluorophore availability, while decreased efficiency at higher concentrations likely results from self-quenching phenomena. It is noteworthy that the plateau observed between 1.0–2.0 mL provides a robust analytical range with minimal sensitivity to small variations in reagent concentration, thereby enhancing method reproducibility.

The time analysis revealed rapid equilibration, with the quenching reaction reaching completion within 3 minutes and maintaining stability for at least 10 minutes (Fig. 4D). This rapid kinetic profile, consistent with the static quenching mechanism and favorable thermodynamic parameters, facilitates high analytical throughput without compromising measurement reliability. Interestingly, the rapid stabilization of the fluorescence signal further supports the proposed static quenching mechanism, as dynamic quenching processes typically exhibit more complex temporal dependencies due to diffusion-controlled interactions.

The optimized conditions (pH 6.0, 1.5 mL buffer, 1.0 mL Rhodamine B solution, 3 minutes reaction time) were subsequently employed for validation experiments, ensuring maximum analytical sensitivity and reproducibility for solriamfetol determination in pharmaceutical and biological matrices.

3.5. Method validation

The analytical performance of the developed spectrofluorimetric method for solriamfetol determination was rigorously validated according to the International Council for Harmonization (ICH) M10 guidelines for bioanalytical procedures. The calibration curve exhibited excellent linearity over the concentration range of 25.0–1000.0 ng mL^{-1} in plasma

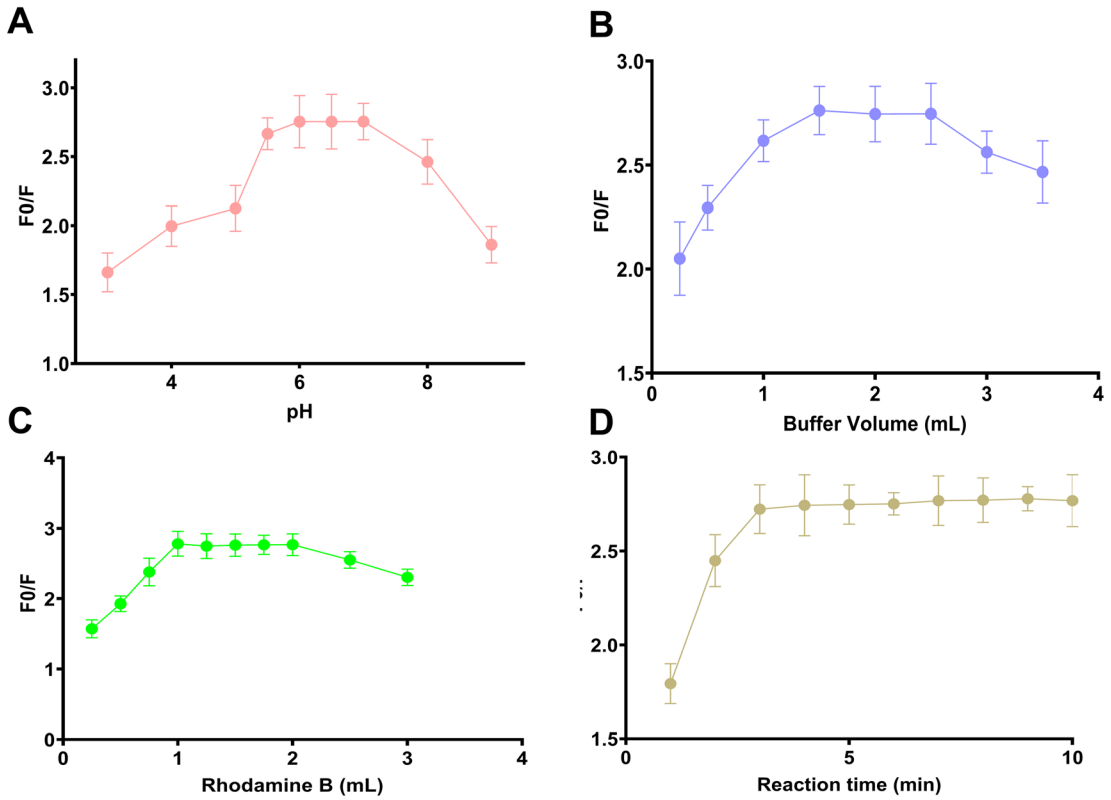

Fig. 4 (A) Effect of pH on fluorescence quenching efficiency demonstrating optimal response at pH 6.0. (B) Influence of buffer volume on analytical response showing maximal signal at 1.5 mL. (C) Fluorophore concentration optimization curve revealing optimal quenching efficiency at 1.0 mL of 0.01% w/v Rhodamine B solution. (D) Reaction time profile demonstrating rapid equilibration within 3 minutes followed by sustained signal stability.

matrix (Fig. 5A), with a coefficient of determination ($r^2 = 0.9991$) demonstrating high correlation between analyte concentration and fluorescence response (Table 2). The limits of detection (LOD) and quantification (LOQ) were calculated as 8.05 ng mL^{-1} and 24.38 ng mL^{-1}, respectively, with a practical LOQ established at 25.0 ng mL^{-1}. The remarkable sensitivity achieved is attributable to the high quantum yield of Rhodamine B and the

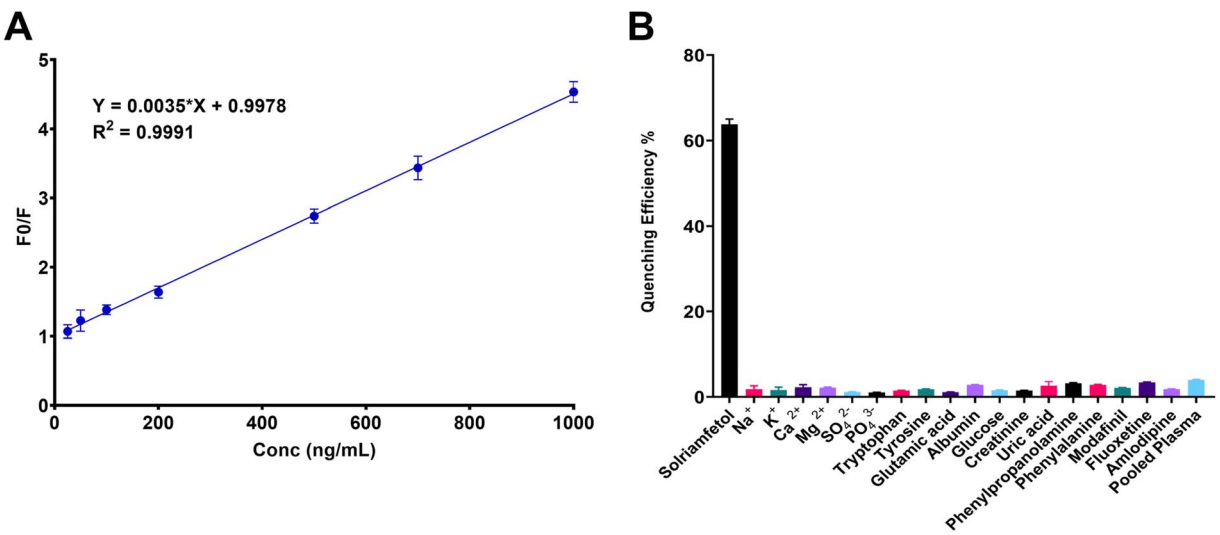

Fig. 5 (A) Standard calibration curve for solriamfetol determination in plasma matrix in aqueous Britton–Robinson buffer (pH 6.0); error bars represent standard deviation of triplicate measurements ($n = 3$). (B) Selectivity assessment against potential interferents showing negligible quenching effect from endogenous plasma constituents compared to solriamfetol under optimized conditions; error bars represent standard deviation of triplicate measurements ($n = 3$).

Table 2 Analytical figures of merit for the validated spectrofluorimetric method demonstrating statistical regression parameters, detection and quantification limits for solriamfetol determination

Parameter	Solriamfetol
Linearity range (ng mL^{-1})	25.0–1000.0
Intercept (a)	0.9978
Slope (b)	0.0035
Coefficient of determination (r^2)	0.9991
SE of intercept (S_a)	0.0239
SE of slope (S_b)	4.72×10^{-5}
LOD (ng mL^{-1})	8.0451
LOQ (ng mL^{-1})	24.3792
LOQ (ng mL^{-1})	25.0

efficient quenching mechanism elucidated through quantum mechanical calculations.

Method accuracy and precision were evaluated at four concentration levels (25, 75, 500, and 750 ng mL^{-1}) across the analytical range using five replicate determinations. Intraday accuracy, expressed as percent recovery, ranged from 96.42 ± 2.56% to 104.84 ± 3.88%, with corresponding precision (% RSD) values between 1.70% and 3.73% (Table S2). Interday accuracy and precision assessment conducted over three consecutive days demonstrated consistent recovery values (97.31 ± 3.42% to 101.60 ± 2.16%) with % RSD values not exceeding 4.56%, indicating excellent method reproducibility. The obtained validation parameters demonstrated full compliance with ICH M10 guidelines for bioanalytical method validation (±15% for nominal concentrations, ±20% at LOQ), confirming the method's suitability for quantitative solriamfetol determination in complex biological matrices.

The selectivity of the developed spectrofluorimetric method was thoroughly investigated by analyzing potential interferents commonly encountered in plasma samples under the optimized analytical conditions. Endogenous plasma constituents including electrolytes (Na^+, K^+, Ca^{2+}, Mg^{2+}, SO_4^{2-}, PO_4^{3-}) and biomolecules (tryptophan, tyrosine, glutamic acid, albumin, glucose, creatinine, uric acid) demonstrated negligible quenching effects on Rhodamine B fluorescence (Fig. 5B). Additionally, structurally related compounds including phenylpropanolamine and phenylalanine exhibited quenching effect percentages of 3.2% and 2.8%, respectively, while commonly co-administered medications including modafinil, fluoxetine, and amlodipine demonstrated quenching effect percentages of 2.1%, 3.4%, and 1.8%, respectively, all negligible compared to 63.8% for solriamfetol at the same concentration. The observed selectivity is attributed to the visible-range excitation at 554 nm circumventing autofluorescence interference, combined with the specific electrostatic complementarity between Rhodamine B's carboxylate moiety and solriamfetol's protonated amine. Furthermore, given solriamfetol's minimal hepatic biotransformation, circulating metabolites are not anticipated to constitute significant interferents in plasma samples. Matrix effect evaluation using three different plasma sources at three concentration levels (75, 500, and 750 ng mL^{-1}) yielded recovery values ranging from 95.08% to 102.99% with coefficient of variation (% CV) values not exceeding 4.01% (Table S3). The slight negative bias observed in some measurements (−0.19% to −4.92%) remained well within acceptable limits, demonstrating minimal matrix interference from endogenous plasma components.

Method robustness was assessed by deliberately introducing small variations in critical experimental parameters: buffer pH (±0.2 units), buffer volume (±0.1 mL), and Rhodamine B volume (±0.1 mL). Analysis of these controlled perturbations at 500 ng mL^{-1} solriamfetol concentration yielded recovery values consistently within 98.22% to 101.43% with standard deviations not exceeding 1.67% (Table S4). This resilience to minor procedural variations reflects the rational optimization of experimental conditions and confirms method reliability under typical laboratory fluctuations.

The quantitative performance of the developed spectrofluorimetric method was further evaluated through direct comparison with LC-MS/MS as the reference method following the validated procedure of Ratnakumari *et al.*[12] Twelve spiked plasma samples prepared at four QC concentration levels (LLOQ QC, LQC, MQC, and HQC) were independently analyzed by both techniques under identical sample preparation conditions. The two methods showed excellent agreement, with Pearson $r = 0.9993$ and $R^2 = 0.9985$ (Fig. S3A, Table S5), both meeting the predefined acceptance criteria of >0.95 and >0.90, respectively. The regression slope of 1.000 (95% CI: 0.973–1.027) and intercept of 7.38 ng mL^{-1} indicated the absence of proportional and constant systematic differences between the spectrofluorimetric and LC-MS/MS measurements. Bland–Altman analysis revealed a mean difference of −7.24 ng mL^{-1} (−7.25%) between the two methods, a value that was not statistically significant ($p = 0.07$), with most of data points falling within the limits of agreement (Fig. S3B). Equivalence testing yielded a 90% CI of 87.0–97.8%, which falls within the ICH M10-specified 80–125% acceptance window (Table S5), confirming that the two methods are analytically equivalent for solriamfetol determination at therapeutically relevant plasma concentrations. These results confirm the suitability of the developed spectrofluorimetric method as a reliable and cost-effective alternative to LC-MS/MS for routine pharmacokinetic monitoring of solriamfetol in human plasma.

3.6. Pharmacokinetic application

The validated spectrofluorimetric method was successfully applied for the determination of solriamfetol concentrations in human plasma following oral administration of a single 75 mg dose to five healthy male volunteers. The mean plasma concentration–time profile revealed a rapid absorption of solriamfetol followed by a multi-exponential decline characteristic of first-order elimination kinetics (Fig. S4). The pharmacokinetic parameters derived from non-compartmental analysis are summarized in Table 3.

The median time to maximum concentration (t_{max}) was calculated as 1.5 h (range: 1–2 h), indicating rapid absorption from the gastrointestinal tract. This value was found to be in agreement with previously reported data by Zomorodi *et al.*

Table 3 Non-compartmental pharmacokinetic parameters following oral administration of solriamfetol (75 mg) to healthy subjects, illustrating the *in vivo* disposition kinetics and bioavailability metrics

Parameters	Mean (% coefficient of variation)
C_{max} (ng mL^{-1})	465 (11.3)
t_{max} (h)[a]	1.5 (1–2)
$t_{1/2}$ (h)	7.6 (20.3)
$AUC_{0\rightarrow t}$ (ng mL^{-1} h^{-1})	4369 (12.4)
$AUC_{0\rightarrow \infty}$ (ng mL^{-1} h^{-1})	4890 (11.2)
V_z/F (L)	171 (27.3)
CL/F (L h^{-1})	15 (10.6)
λ_z (h^{-1})	0.09 (20.8)

[a] Expressed as median (range).

where a median t_{max} of 1.3 h (range: 0.5–2.0 h) was reported in subjects with normal renal function following a 75 mg dose.[4] The mean maximum plasma concentration (C_{max}) was determined to be 465 ng mL^{-1} (CV = 11.3%), demonstrating consistent absorption characteristics with minimal inter-subject variability. The area under the plasma concentration–time curve from zero to the last measurable concentration ($AUC_{0\rightarrow t}$) and extrapolated to infinity ($AUC_{0\rightarrow \infty}$) were determined to be 4369 ng h mL^{-1} (CV = 12.4%) and 4890 ng h mL^{-1} (CV = 11.2%), respectively, indicative of complete absorption and adequate characterization of the plasma concentration–time profile.

The calculated apparent volume of distribution (V_z/F = 171 L, CV = 27.3%) suggests moderate tissue distribution, which corresponds closely with the value reported in subjects with normal renal function (163.9 L, CV = 14.5%) by Zomorodi *et al.* in their renal impairment investigation.[4] This correlation confirms the ability of the developed spectrofluorimetric method to accurately characterize the distribution phase of solriamfetol pharmacokinetics. The moderate volume of distribution suggests partial distribution into tissues beyond the vascular compartment.

The apparent elimination half-life ($t_{1/2}$) was calculated as 7.6 h (CV = 20.3%), which compares favorably with the reported value of 7.6 h (CV = 67.7%), suggesting consistent characterization of the elimination phase with improved precision using the developed spectrofluorimetric method.[4] The terminal elimination rate constant (λ_z) was determined to be 0.09 h^{-1} (CV = 20.8%), indicating uniform elimination kinetics across the study population. Furthermore, the apparent clearance determined in our study (CL/F = 15 L h^{-1}, CV = 10.6%) aligns with previously reported values,[5] thereby confirming the reliability of our quantification methodology for evaluating the elimination characteristics of solriamfetol.

The high sensitivity and selectivity that were achieved by this spectrofluorimetric method for accurate characterization of the pharmacokinetic parameters of solriamfetol. Also, the low variability in estimated parameters (CV < 30% for all primary parameters), which was found to be comparable to or better than previously reported analytical methodologies for solriamfetol determination, suggests high methodological robustness and reproducibility across the concentration range encountered during therapeutic monitoring. Hence, this method offers a simpler, more environmentally sustainable alternative to chromatographic techniques while maintaining comparable analytical performance characteristics for solriamfetol quantification in biological matrices.

3.7. Comparison with reported analytical methods

The comprehensive analytical methodology developed in this study for the determination of solriamfetol in plasma samples based on Rhodamine B fluorescence quenching was comparatively evaluated against previously reported analytical approaches. A detailed assessment of the analytical performance parameters is presented in Table 4, enabling critical comparison across various methodologies.

The HPLC technique employing polar organic mode with Lux Amylose-1 column reported by Köteles *et al.*[10] exhibited a relatively high limit of detection (2.4 μg mL^{-1}) and quantification (8 μg mL^{-1}), rendering it suitable primarily for bulk pharmaceutical substance analysis rather than trace-level determination in biological matrices. While this method offered adequate chromatographic resolution for enantiomeric purity evaluation, its μg mL^{-1}-range sensitivity limits its applicability for pharmacokinetic investigations.

The UPLC-UV method developed by Al-Rifai *et al.*[11] for impurity profiling demonstrated variable sensitivity across different impurities and required a relatively lengthy analysis time (22 min). Although this method provided comprehensive impurity separation, its detection capabilities were insufficient for quantifying solriamfetol at low concentrations in complex biological matrices.

The LC-MS/MS method reported by Ratnakumari *et al.*[12] demonstrated high sensitivity with an impressively low LOD (11.12 pg mL^{-1}) and LOQ (33.70 pg mL^{-1}), making it highly suitable for plasma sample analysis. While this method offers excellent sensitivity and a short analysis time (3 min), it necessitates sophisticated instrumentation, complex sample preparation involving protein precipitation, and substantial technical expertise, factors that may constrain its routine implementation in resource-limited settings.

The capillary electrophoresis method utilizing sulfated γ-cyclodextrin reported by Fejős *et al.*[13] achieved baseline separation within 7 minutes and demonstrated applicability for pharmaceutical tablet analysis. However, with a LOQ of 5 μg mL^{-1}, this technique offers limited sensitivity for plasma sample analysis, where sub-μg mL^{-1} concentrations are frequently encountered in pharmacokinetic studies.

The spectrofluorimetric method recently reported by Kamel *et al.*,[9] based on intrinsic fluorescence measurement, demonstrated good sensitivity (LOD: 3.2 ng mL; LOQ: 9.8 ng mL^{-1}) and a wide linear range (10–1800 ng mL^{-1}). However, excitation at 260 nm falls within a spectral region where numerous biomolecules exhibit autofluorescence, potentially compromising selectivity in complex biological matrices.

In contrast, the present spectrofluorimetric method based on Rhodamine B fluorescence quenching offers several distinct

Table 4 Comparative analytical performance characteristics of various instrumental techniques for solriamfetol determination

Analytical method	Detection system/material	Linear range	LOD	LOQ	Analysis time	Sample matrix	Reference
HPLC (polar organic mode)	UV detection at 210 nm, Lux Amylose-1 column	8–160 μg mL^{-1} [a]	2.4 μg mL^{-1}	8 μg mL^{-1}	6 min	Pharmaceutical substance	Köteles *et al.* (2020)[10]
UPLC-UV	UV detection at 210 nm, Kinetex polar C18 column	50–3000 ng mL^{-1} [b]	0.4–29.0 ng mL^{-1} [c]	1.1–89.0 ng mL^{-1} [c]	22 min	Pharmaceutical substance (impurity analysis)	Al-Rifai *et al.* (2023)[11]
LC-MS/MS	Xterra MS C18 column with CEM array detector	5–500 ng mL^{-1}	11.12 pg mL^{-1}	33.70 pg mL^{-1}	3 min	Human plasma	Ratnakumari *et al.* (2021)[12]
Capillary electrophoresis	UV detection at 210 nm, sulfated γ-cyclodextrin (S-γ-CD)	5–60 μg mL^{-1}	Not reported	5 μg mL^{-1}	7 min	Pharmaceutical tablets	Fejős *et al.* (2021)[13]
Spectrofluorimetry	Intrinsic fluorescence ($\lambda_{ex}/\lambda_{em}$ = 260/522 nm) in ammonium acetate buffer (pH 4)	10–1800 ng mL^{-1}	3.2 ng mL^{-1}	9.8 ng mL^{-1}	Not specified	Pharmaceutical dosage form, plasma, urine	Kamel *et al.* (2024)[9]
Spectrofluorimetry	Quenching of Rhodamine B ($\lambda_{ex}/\lambda_{em}$ = 554/578 nm)	25–100 ng mL^{-1}	8.1 ng mL^{-1}	24.38 ng mL^{-1}	3 min	Plasma	Current work

[a] For *S*-enantiomer in presence of 8000 μg mL^{-1} *R*-solriamfetol. [b] For impurity analysis (0.003–0.3% of nominal concentration). [c] Values vary by specific impurity.

advantages. The utilization of visible light excitation (λ_{ex} = 554 nm) circumvents interference from endogenous biomolecule fluorescence commonly encountered in biological samples, enhancing method selectivity. Additionally, the current method provides excellent sensitivity (LOD: 8.1 ng mL^{-1}; LOQ: 24.38 ng mL^{-1}) comparable to other spectrofluorimetric approaches, while maintaining a relatively fast analysis time (3 min). Although the linear range (25–1000 ng mL^{-1}) is narrower than that reported by Kamel *et al.*, it adequately encompasses the concentration range necessary for pharmacokinetic profiling, as evidenced by the successful application to volunteer plasma samples.

The high sensitivity combined with simple sample preparation, rapid analysis time, and utilization of environmentally benign reagents positions this Rhodamine B fluorescence quenching method as an excellent alternative to chromatographic techniques for routine pharmacokinetic investigations and therapeutic drug monitoring of solriamfetol in clinical settings.

4. Conclusion and future directions

This study presents a novel spectrofluorimetric method for solriamfetol determination in plasma based on its quenching effect on Rhodamine B fluorescence. Initially, comprehensive spectral investigations were conducted, revealing characteristic absorption maxima at 554 nm for Rhodamine B and strong emission at 578 nm, providing the spectroscopic basis for the analytical methodology. Subsequently, mechanistic elucidation through Stern–Volmer analysis revealed static quenching (K_{sv} = 7.95 × 10^5 L mol^{-1}) with a thermodynamically favorable interaction (ΔG = −33.66 kJ mol^{-1}) and 1 : 1 stoichiometry. Furthermore, quantum mechanical calculations confirmed electrostatic interactions between solriamfetol's protonated amine and Rhodamine B's carboxylate (intermolecular distance 3.02 Å), with negative binding energy (ΔE = −0.041229 hartree). Optimization of experimental parameters including pH (6.0), buffer volume (1.5 mL), Rhodamine B concentration (1.0 mL of 0.01% w/v solution), and reaction time (3 minutes) was systematically conducted to maximize analytical sensitivity. Consequently, validation according to ICH M10 guidelines demonstrated excellent linearity (r^2 = 0.9991) across 25.0–1000.0 ng mL^{-1} with high sensitivity (LOD = 8.05 ng mL^{-1}, LOQ = 24.38 ng mL^{-1}) and precision (% RSD < 4.56%). The method's primary advantages include: (1) visible light excitation (λ_{ex} = 554 nm) circumventing biomolecular autofluorescence interference commonly associated with UV excitation; (2) rapid analysis time (3 minutes) enabling high throughput screening; (3) simplified sample preparation relative to chromatographic techniques; (4) environmentally benign reagents in accordance with green analytical chemistry principles. The method was successfully applied to pharmacokinetic profiling in human volunteers, yielding clinically relevant parameters ($t_{1/2}$ = 7.6 h, C_{max} = 465 ng mL^{-1}, t_{max} = 1.5 h).

Future investigations should address certain limitations of the current methodology. Primarily, while visible excitation minimizes matrix interference, protein binding effects in highly

concentrated plasma samples require further investigation. Additionally, development of molecularly imprinted polymers specifically designed for solriamfetol recognition could improve selectivity in complex matrices, potentially lowering detection limits through pre-concentration. Moreover, adaptation to near-infrared fluorophores could further enhance selectivity by eliminating residual biological matrix interference. Beyond these analytical improvements, the interaction mechanism and analytical framework established in this work may further inspire the development of novel bioassays, point-of-care diagnostic platforms, and emerging sensing technologies for solriamfetol and structurally related controlled substances in diverse clinical and forensic applications. It is acknowledged that for anti-doping surveillance programs requiring ultra-trace detection capabilities at pg mL^{-1} concentration levels, more sensitive analytical platforms such as LC-MS/MS would be more appropriate; however, the developed method remains well-suited for therapeutic drug monitoring and pharmacokinetic investigations where analyte concentrations fall within the therapeutically relevant ng mL^{-1} range.

Conflicts of interest

There are no conflicts to declare.

Data availability

The authors confirm that the data supporting the findings of this study are available within the article and its supplementary information (SI). Any additional data are available from the corresponding author upon reasonable request. Supplementary information is available. See DOI: https://doi.org/10.1039/d6ra02388f.

Acknowledgements

The authors gratefully acknowledge Princess Nourah bint Abdulrahman University, Riyadh, Saudi Arabia for supporting this work through Princess Nourah bint Abdulrahman University Researchers Supporting Project number (PNURSP2026R466), Princess Nourah bint Abdulrahman University, Riyadh, Saudi Arabia.

References

1 A. Markham, *Drugs*, 2019, **79**, 785–790.
2 M. J. Thorpy, C. Shapiro, G. Mayer, B. C. Corser, H. Emsellem, G. Plazzi, D. Chen, L. P. Carter, H. Wang, Y. Lu, J. Black and Y. Dauvilliers, *Ann. Neurol.*, 2019, **85**, 359–370.
3 M. G. Baladi, M. J. Forster, M. B. Gatch, R. B. Mailman, D. L. Hyman, L. P. Carter and A. Janowsky, *J. Pharmacol. Exp. Ther.*, 2018, **366**, 367–376.
4 K. Zomorodi, D. Chen, L. Lee, K. Lasseter and T. Marbury, *J. Clin. Pharmacol.*, 2019, **59**, 1120–1129.
5 K. Zomorodi, M. Kankam and Y. Lu, *Clin. Ther.*, 2019, **41**, 196–204.
6 S. C. Veasey, C. Guilleminault, K. P. Strohl, M. H. Sanders, R. D. Ballard and U. J. Magalang, *Sleep*, 2006, **29**, 1036–1044.
7 J.-L. Pépin, V. Viot-Blanc, P. Escourrou, J.-L. Racineux, M. Sapene, P. Lévy, B. Dervaux, X. Lenne and A. Mallart, *Eur. Respir. J.*, 2009, **33**, 1062–1067.
8 P. K. Schweitzer, R. Rosenberg, G. K. Zammit, M. Gotfried, D. Chen, L. P. Carter, H. Wang, Y. Lu, J. Black, A. Malhotra, K. P. Strohl, A. Blackman, C. George, C. Shapiro, C. Shapiro, H. Benes, I. Fietze, G. Mayer, P. Young, G. J. Lammers, M. Ahmed, A. Ajayi, J. Andry, R. Artal, B. Bastani, R. Bogan, B. Corser, C. Drake, H. Emsellem, M. Erman, N. Feldman, N. Foldvary, M. Gotfried, J. Hudson, L. Krahn, D. Lorch, A. Malhotra, J. Maynard, E. Mignot, M. Neeb, J. Ojile, A. T. Perkins, R. Rosenberg, A. Roy, P. Sahota, R. B. Sangal, A. Schreiber, P. Schweitzer, R. Steele, T. Stern, T. Stern, S. Stolz, K. Strohl, T. Swick, T. J. Swick, S. G. Thein, R. Thomas, M. Thorpy, T. Weaver, K. Wilks, D. Winslow, P. Wylie, G. Zammit and P. Zee, *Am. J. Respir. Crit. Care Med.*, 2019, **199**, 1421–1431.
9 M. Z. Kamel, H. Z. Yamani, L. A. Hussein and Y. A. Trabik, *Microchem. J.*, 2024, **207**, 111930.
10 I. Köteles, M. Foroughbakhshfasaei, M. Dobó, M. Ádám, I. Boldizsár, Z.-I. Szabó and G. Tóth, *Chromatographia*, 2020, **83**, 909–913.
11 N. Al-Rifai, A. Alshishani, F. Darras, O. Taha, S. Abu-Jalloud, L. Shaghlil and Y. Al-Ebini, *J. Pharm. Anal.*, 2023, **13**, 403–411.
12 P. Ratnakumari, N. Kannappan and P. Premkumar, *Int. J. Life Sci. Pharma Res.*, 2022, **11**, 129–138.
13 I. Fejős, G. Tóth, B. Várnai, Z. I. Szabó, I. Köteles, M. Malanga and S. Béni, *Electrophoresis*, 2021, **42**, 1818–1825.
14 R. M. Alnemari, M. H. Abduljabbar, Y. S. Althobaiti, S. Alshehri, F. M. Almutairi, H. A. Shmrany, E. S. Alatwi, A. Serag and A. H. Almalki, *J. Photochem. Photobiol., A*, 2025, **465**, 116357.
15 A. S. Alqahtani, F. M. Almutairi, M. M. Aldhafeeri, Y. S. Althobaiti, M. H. Abduljabbar, A. Serag and A. H. Almalki, *Spectrochim. Acta, Part A*, 2025, **327**, 125342.
16 R. A. Felemban, M. H. Abduljabbar, R. M. Alnemari, R. M. Alzhrani, Y. S. Althobaiti, M. F. Aldawsari, A. Serag and A. H. Almalki, *RSC Adv.*, 2025, **15**, 8855–8866.
17 A. Serag, M. H. Abduljabbar, Y. S. Althobaiti, R. M. Alnemari, F. M. Almutairi, M. M. Aldhafeeri and A. H. Almalki, *Microchem. J.*, 2025, **208**, 112523.
18 A. H. Almalki, M. H. Abduljabbar, R. M. Alnemari, M. E. Alosaimi, S. I. Alaqel and A. Serag, *Microchem. J.*, 2024, **205**, 111381.
19 M. H. Abduljabbar, R. M. Alnemari, A. H. Almalki, M. Alqarni, M. A. Abdel Rahman and A. Serag, *Luminescence*, 2024, **39**, e4928.
20 S. O. Fakayode, C. Lisse, W. Medawala, P. N. Brady, D. K. Bwambok, D. Anum, T. Alonge, M. E. Taylor, G. A. Baker and T. F. Mehari, *Appl. Spectrosc. Rev.*, 2024, **59**, 1–89.

21 O. M. Obukhova, N. O. Mchedlov-Petrossyan, N. A. Vodolazkaya, L. D. Patsenker and A. O. Doroshenko, *Colorants*, 2022, **1**, 58–90.
22 S. Bakkialakshmi, P. Selvarani and S. Chenthamarai, *Spectrochim. Acta, Part A*, 2013, **105**, 557–562.
23 I. Guideline, *ICH Harmonised Guideline*, Geneva, Switzerland, 2022.
24 Y. Zhang, M. Huo, J. Zhou and S. Xie, *Comput. Methods Progr. Biomed.*, 2010, **99**, 306–314.